Scientific Research Publishing

World Journal of Nuclear Science and Technology, 2025, 15(4), 135-153
https://www.scirp.org/journal/wjnst
ISSN Online: 2161-6809
ISSN Print: 2161-6795

Modulation of the Excitation Characteristics of the Na Atom in Quantum Plasma via Spherical Confinement and Plasma Screening

Louis Gomis*, Clement Diatta, Ibrahima Gueye Faye, Yandé Diouf, Mamadou Coulibaly, Rama Gomis, Attitchou Kossi

Laboratory of Plasma Physics and Interdisciplinary and Research, Department of Physics, Faculty of Science and Technology, University Cheikh Anta Diop, Dakar, Senegal
Email: *lgomis73@yahoo.fr

How to cite this paper: Gomis, L., Diatta, C., Faye, I.G., Diouf, Y., Coulibaly, M., Gomis, R. and Kossi, A. (2025) Modulation of the Excitation Characteristics of the Na Atom in Quantum Plasma via Spherical Confinement and Plasma Screening. *World Journal of Nuclear Science and Technology*, **15**, 135-153.
https://doi.org/10.4236/wjnst.2025.154010

Received: September 21, 2025
Accepted: October 28, 2025
Published: October 31, 2025

Abstract

The generalized oscillator strengths (GOS) as a function of squared momentum transfer are calculated within the Bethe-Born approximation for the dipole $3s \to 3s^o(3p, 4p)$, quadrupole $3s \to 3s^o(3d, 4d)$, and octupole $3s \to 3s^o(4f, 6f)$ transitions of the sodium atom under spherical confinement and quantum plasma conditions. These GOS values for multiple strengths ($\ell = 1, 2, 3$) are computed using initial and final state wave functions obtained from the work of Bahar by solving the wave equation, including the more general plasma model potential (MGPM). Their results are reported for both spherical confinement with fixed radius R and different plasma conditions defined by a set of plasma shielding parameters (a, b, D), two of which are fixed while the other is varied. The analysis elucidates that the competition between both interactions, due to the combined effect of these parameters, leads to various behaviors of the GOS for each multipole strength considered in the present work. According to the present calculations, additional GOS maxima emerge in the observed GOS curves, revealing the influence of the parameter b. We also note that, apart from a second maximum that appears near a small q^2 region for some cases of D and a, the positions of the GOS maxima for quadrupole ($3s \to 3s^o(3d, 4d)$) and octupole ($3s \to 3s^o(4f, 6f)$) transitions shift towards greater squared momentum transfer with the increment in D, while they move to smaller squared momentum transfer as the parameter a increases.

Keywords

Quantum Plasma, Atomic Sodium, Dipole Oscillator Strength, Generalized Oscillator Strength

1. Introduction

Considerable interest in the study of atomic processes has attracted the attention of many researchers due to the ever-increasing need for cross-section data in many fields, such as astrophysics, plasma physics, ionized gases, and solid-state physics. In the case of electron-impact inelastic collisions of atomic systems, the cross section can be suitably studied within the Bethe-Born approximation (BBA) through the generalized oscillator strength (GOS). The generalized oscillator strength, or equivalently the cross section, is used to explore excitation dynamics. Most studies based on the generalized oscillator strength have shown that the data obtained for atomic systems in plasma environments are likely to differ from those of free atomic systems due to the screening effect of the surrounding plasma particles.

Despite being a simple single-valence-electron system, the sodium atom is regarded as an ideal test case for understanding the influence of strong correlation effects and external environmental conditions (such as plasma, magnetic fields, or confinement) on atomic structure. Therefore, theoretical investigations on sodium are of great importance for elucidating how electron-electron interactions, energy levels, and transition probabilities are modified in multi-electron atoms. In addition, the optical transition properties of sodium serve as key references in experimental applications, such as laser cooling and atomic clock technologies [1]. Moreover, the well-known sodium D-lines observed in astrophysical environments, such as stellar atmospheres and cometary tails, play a crucial role in modeling ionization processes and radiative transfer phenomena [2]. Consequently, a detailed investigation of the behavior of sodium in plasma environments provides valuable insights not only for fundamental atomic physics but also for various applied research fields. As aforementioned above, the investigation of the dynamic processes of atomic sodium is both important and interesting, since sodium exists in comets and in the atmosphere. In addition to this presence, there is also observational evidence for the effect of plasma on neutral sodium clouds and for the nature of the sodium plasma created by the ionization of sodium emitted into Jupiter's environment, as reported in the presentation of Eviatar *et al.* [3] in 1976. Many theoretical studies on the generalized oscillator strength of the free sodium atom, using approaches such as the R-Matrix method [4] [5] and the Random Phase Approximation with Exchange (RPAE) [6], have highlighted the significant role of electron-electron interactions due to their strong intensity. Calculations of the dipole and generalized oscillator strengths have also been carried out for transitions of atomic sodium in a plasma environment, using the radial wavefunctions of the ground and excited states obtained by solving the radial Schrödinger equation that includes the interaction potential within the model potential framework. Sahoo *et al.* [7] determined the photoionization cross sections of sodium and lithium atoms in a plasma environment by considering the Debye-Hückel model potential, which simulates the multielectron core interaction with the single valence electron. In the case of atomic sodium, it was found that the Cooper minimum shifts toward

higher energies as the plasma screening increases. A few years later, theoretical investigations of the oscillator strengths and dipole polarizabilities of the $3s$ and $3p$ states of sodium embedded in weakly coupled plasma were carried out by Qi *et al.* [8] under the first Born approximation, using radial wavefunctions obtained from a pseudopotential model to modify the $3s$ valence state. Taking advantage of a model potential formalism within the relativistic Hartree-Fock-Slater (HFS) framework, Madhulika *et al.* [9] investigated the effect of the plasma environment on the structure and properties of atomic sodium and lithium. Their results show that plasma screening significantly affects the aforementioned observables. For example, they reported that inclusion of the Debye screening in the HFS effective potential mainly causes variations in the oscillator strengths. Martinez-Flores [10] studied the effects of plasma screening on fast charged-particle impact excitation of the sodium atom using the Bethe-Born approach through the generalized oscillator strength. The calculations of Martinez-Flores [10] employed the wavefunctions of the sodium atom before and after collision, obtained using both the Debye-Hückel screened (DHS) potential model and the exponential cosine screened Coulomb (ECSC) potential model, to provide GOS data by applying the length-form formalism. This study revealed that the exponential cosine screened Coulomb potential model yields a much stronger decrease in the GOS values for sodium transitions compared to the Debye-Hückel screened potential. These works are among the studies that have successfully incorporated plasma screening effects into the atomic structure and dynamic processes of sodium, such as dipole and generalized oscillator strengths, dipole polarizabilities, and photoionization cross sections.

In light of the explanations so far, to the best of our knowledge, it is clear that, to date, no study has been conducted on the generalized oscillator strength as a function of the squared momentum transfer for spherically confined atomic sodium embedded in quantum plasma. When both the quantum plasma environment and the effect of spherical confinement act simultaneously, they cause significant modifications in atomic binding energies, transition probabilities, and dipole, quadrupole, and octupole responses. Therefore, revealing how the generalized oscillator strength evolves as a function of the squared momentum transfer provides a new perspective for both atomic structure theory and research on plasma diagnostics and controlled fusion. Such an analysis allows for a quantitative determination of the rearrangement of energy levels under high-density plasma conditions, the suppression or enhancement tendencies of optical transitions, and the magnitude of quantum effects near the ionization threshold. Moreover, the data obtained in this study can directly support radiation-transport models of atoms in dense plasmas, assist in the interpretation of spectral-line shifts, and improve predictions of the optoelectronic properties of nanostructured confined systems. These applications underline the practical importance of filling the identified research gap and further motivate the relevance of our calculations. These potentially significant outcomes have constituted a strong motivation for

the present study. The main purpose of this paper is to investigate, in the length form, the generalized oscillator strength for some valence-shell transitions of atomic sodium in this extreme environment. To deal with the GOS, we need atomic sodium energies and wavefunctions generated under the combined influence of both spherical confinement and quantum plasma. The wavefunctions considered here were calculated in the work of Bahar by solving the Schrödinger equation that includes the more general plasma model (MGPM) potential, which simultaneously accounts for strong particle correlations in the quantum plasma and the strong confinement effect. The initial and final state wavefunctions obtained numerically in Bahar's calculations are used in this work to provide several multipole GOSs for the excitations to $3s^o\left(3p,3d,4p,4d,4f,6f\right)$.

We organized this paper as follows. The next section is the review of the length formulation of GOS and the more general plasma model potential described in details in Bahar's work. Section 3 has presented the application of MGPM potential for three different cases in which we also have different values and the results of our calculations for dipole and generalized oscillator strengths are given and discussed. Finally, we conclude in the last section of this paper where atomic units were used, unless explicitly indicated otherwise.

2. Theoretical Model and Procedure

When the charged projectile involved in the scattering process is moving sufficiently fast and in a non-relativistic frame, the differential cross section for inelastic collisions of the atomic system, whose state changes from the initial one (i) to the final one (f), is obtained from the transition amplitude by Fermi's Golden Rule [11]:

$$\frac{\mathrm{d}\sigma_{if}}{\mathrm{d}\Omega}=\frac{2\pi}{v_i}\left|U_{if}\right|^2\rho\left(E_f\right), \tag{1}$$

where v_i is the initial velocity of the incident charged particle. According to Born approximation, the matrix element for transition from initial state to final state U_{if} can here be written as:

$$U_{if}=\Psi_{fp_j}U\Psi_{ip_i} \tag{2}$$

with Ψ_{fp_j} and Ψ_{ip_i} are respectively the eigenfunctions of the system before and after the collision, p_j and p_i are final and initial momentum of the scattered and incident particle. In this Equation (2), U represents the coulombic interaction operator. It is well known that the density $\rho\left(E_f\right)$ of final states per unit energy E_f per unit solid angle $\mathrm{d}\Omega$ into which the scattered particle goes, may have the form:

$$\rho\left(E_f\right)=\frac{p_j^2}{\left(2\pi\right)^3}\frac{\mathrm{d}\rho_f}{\mathrm{d}E_f} \tag{3}$$

with $\frac{\mathrm{d}E_f}{\mathrm{d}p_f}=v_f$ defining the velocity of the scattered charged particle. By treating

the fast charged particle before and after the collision as plane waves and then evaluating first the integration over its radial coordinate, we obtain, in the Born approximation, the differential cross section, calculated in the lowest order under interaction U between the particle and the target atom. This differential cross section can be expressed as a function of the momentum transfer q by the following formula:

$$\mathrm{d}\sigma_{if} = \frac{8\pi \mathrm{d}q}{q^3 v^2}\left|\sum_{j=1}^{N}\left\langle \Psi_f \left| \mathrm{e}^{i\boldsymbol{q}\cdot\boldsymbol{r}} \right| \Psi_i \right\rangle\right|^2. \tag{4}$$

The conditional probability that the atom makes the transition upon receiving a momentum transfer q is given by the square of the matrix element which reflects the response of the target atom and is known as the inelastic scattering form factor. Widely used in nuclear and particle physics, Bethe introduces, in the determination of the stopping power of matter, a new quantity which is slightly different from the inelastic-scattering form factor. This quantity proportional to the inelastic-scattering form factor is known as the generalized oscillator strength [12]:

$$G_{ij}(\omega, q) = \frac{2\left(E_f - E_i\right)}{q^2}\left|\sum_{j=1}^{N}\left\langle \Psi_f \left| \mathrm{e}^{i\boldsymbol{q}\cdot\boldsymbol{r}} \right| \Psi_i \right\rangle\right|^2. \tag{5}$$

By considering singlet electron transitions from the state denoted by m to excited state denoted by n, Equation (5) simplifies considerably, reducing to

$$g_{mn}(\omega, q) = \frac{2\omega_{nm}}{q^2}\left|\left\langle \Psi_n \left| \mathrm{e}^{i\boldsymbol{q}\cdot\boldsymbol{r}} \right| \Psi_m \right\rangle\right|^2, \tag{6}$$

where ψ_n and ψ_m are respectively the final and initial state functions with its corresponding eigenvalue energies ε_n and ε_m, when the energy conservation law $\omega_{nm} = \varepsilon_n - \varepsilon_m$ is satisfied. Owing to the presence of just the state functions being normalized anti-symmetrized products of spatial and spins factors and for an electron operator in the spherical wave expansion, Equation (6) becomes

$$g_{mn}(\omega, q) = \sum_k g_{mn}^k(\omega, q) \tag{7}$$

with g_{mn}^k being ℓ multipole GOS and can be given as follows [13]:

$$\begin{aligned} g_{mn}^k(\omega, q) = {} & \frac{2\omega_{nm} N_m (2k+1)}{q^2 (2\ell_m + 1)}(2\ell_n + 1)(2\ell_m + 1) \\ & \times \left| \begin{pmatrix} \ell_n & k & \ell_m \\ 0 & 0 & 0 \end{pmatrix} \int_0^\infty P_{n_m \ell_m}(r)\, j_k(qr)\, P_{n_n \ell_n}(r)\, \mathrm{d}r \right|^2 \end{aligned} \tag{8}$$

where N_m is the number of electrons in the excited state and k the total angular momentum of the electron-hole pair which satisfies the triangular rule $\left|\ell_m + \ell_n\right| \geq k \geq \left|\ell_m - \ell_n\right|$. We also note that here $j_k(qr)$ is the spherical Bessel function of the first kind. $P_{m,\ell_n}(r)$ and $P_{n,\ell_n}(r)$ being respectively, the initial and final normalized reasonable physical radial functions of quantum plasma-immersed compressed sodium atom, calculated in the study of Bahar by considering

in the numerical resolution of the radial Schrödinger equation, the model potential known as the more general plasma model potential (MGPM) and given in the following form in the paper of Bahar [14].

$$V_{\mathrm{MGPM}}(r,Z,D,a,b)=V_{\mathrm{model}}(r,Z)(1+br)\times \mathrm{e}^{-\frac{r}{D}}\cos\left(\frac{ar}{D}\right), \tag{9}$$

where $V_{\mathrm{model}}(r,Z)$ is the model potential well defined in his paper [14] and a,b and D defining as the plasma shielding parameters: a the oscillatory screening parameter controlling the frequency cosine oscillation, b is the linear correction parameter which adjusts the potential at short-distance in order to make it more accurate near the nucleus or for close particles interactions, and D the screening length which determines how fast the potential decreases with distance. Then, these radial wavefunctions of sodium atom surrounded by the sphere of radius $R=25$, obtained from the work of Bahar are employed to compute the GOS for the excitations to $3s^0(3p,4p,3d,4d,4f,6f)$. Computed data from Equation (8) by using Matlab software are presented and compared with the theoretical and experimental results available in the literature.

3. Results

As one can see from Equation (9), there are three different screening parameters which permit this model potential to describe adequately the effective interaction in many-electron atomic phenomena. For the purposes of the present work, the radial wavefunctions generated from the code of Bahar for some special values of a,b,D and $R=25$, as well as the spherical confining box radius will be used in Equation (8) to compute the partial generalized oscillator strength. The results of partial contribution transition GOS are presented for three cases in which one various of the shielding parameters and two others have different values.

The oscillator strength values $D=100,50,30$, and 20 have also been calculated for the case of $a=1$, $b=0$, and $R\to\infty$, considering the dipole transitions $3s\to 3s^0(3p,4p)$, and the results are presented in **Table 1**. This table also includes the available oscillator strength data for these transitions obtained from theoretical calculations [9] [11] [15] [16]. For comparison purposes, the oscillator strength values corresponding to these dipole transitions are provided here for the sodium atom embedded in a Debye-Hückel screened plasma environment [9] and under the exponential-cosine-screened Coulomb potential [11]. In the theoretical studies [15] [16], other oscillator strength values obtained from inelastic scattering processes of the sodium atom in plasma environments were reported using the generalized oscillator strength (GOS) expressions in the length [17] and velocity [18] formulations. In those works, in addition to the earlier methods incorporating plasma screening effects, an additional investigation was performed within the framework of the Random Phase Approximation with Exchange (RPAE) [19] [20], which takes into account the correlations among the electrons of the sodium

atom. For comparison with these references, the limit $a=1$, $b=0$, and $R\to\infty$ of the MGPM potential is considered. In the present work, it is found that the results obtained using the Exponential Screened Coulomb Potential (ECSC) without spherical confinement are in very good agreement with those of other researchers. This consistency is highly significant in terms of validating the accuracy of our computational model and methodology.

Table 1. Oscillator strength for dipole $3s\to 3s^0(3p,4p)$ transitions for Na atom under quantum plasma ($a=1$, $b=0$, $R\to\infty$).

Transition	$3s\to 3s^0 3p$			$3s\to 3s^0 4p$		
D	Present work	[9] [15] [16]	[11]	Present work	[9] [15] [16]	[11]
100	0.99876	1.01700[k]	0.98127	0.013999	0.01450[k]	0.01416
	0.98314	0.98199[h]	0.98263	0.014001	0.01451[h]	0.01413
	0.98569	0.99810[l]	0.98401	0.014014	0.01398[l]	0.01416
	0.98701	0.96000[k]	0.98459	0.014012	0.01371[k]	0.01401

Reference [7]; Reference [19]: RPAE-V results; **Reference [20]**: RPAE-L results.

3.1. As a Function of *D*

Figure 1 shows our findings for generalized oscillator strengths of the $3s\to 3s^0(3p,3d,4p,4d,4f,6f)$ transitions for $b=0.5$, $a=1$, $R=25$ and four different values of D which are $D=10,30,100$ and 250. While when the squared momentum transfer going from the value in the q^2 region of 1 - 2 au, GOS curves converge to zero for all screening parameter D considered above. As seen in the panels a) and b) of this **Figure 1**, the dipole oscillator strengths (DOS) for excitations to $3s^0(3p,4p)$ decrease with increasing of squared momentum transfer q^2. From **Figure 1(a)**, DOS curve for $D=10$ is below those depicting the calculated results with $D=100$ and 250 which are close together when the squared momentum transfer $q^2\le 0.16254$. Above this q^2 value, the DOS picture for $D=10$ is above those obtained in the cases of $D=100$ and 250. This may be explained by the fact that the delicate interference of the oscillations in the radial part of the initial and final state wavefunctions in the cases of $D=100$ and 250, leads to their poor overlap by growth of q^2. This can be explained by the fact that a stronger attractive potential increases the curvature of the wavefunction, thereby confining it to a smaller spatial region. The present calculations give the DOS for the excitation to $3s^0 3p$ as $q^2\to 0$ the values 1.07862, 1.73467 and 1.87634 for $D=10,100$ and 250, respectively. All these values are greater than the reported value 0.97976 of Martinez-Flores [12] in the framework of free case and the free value ($D\to\infty$) of the dipole oscillator strength which reaches 0.9758 listed in the paper of Li *et al.* [21] and 0.97981 listed in the paper of Qi *et al.* [8]. It is also clear that there is a difference between our calculated values and the measured oscillator strength with value of 0.9820 for

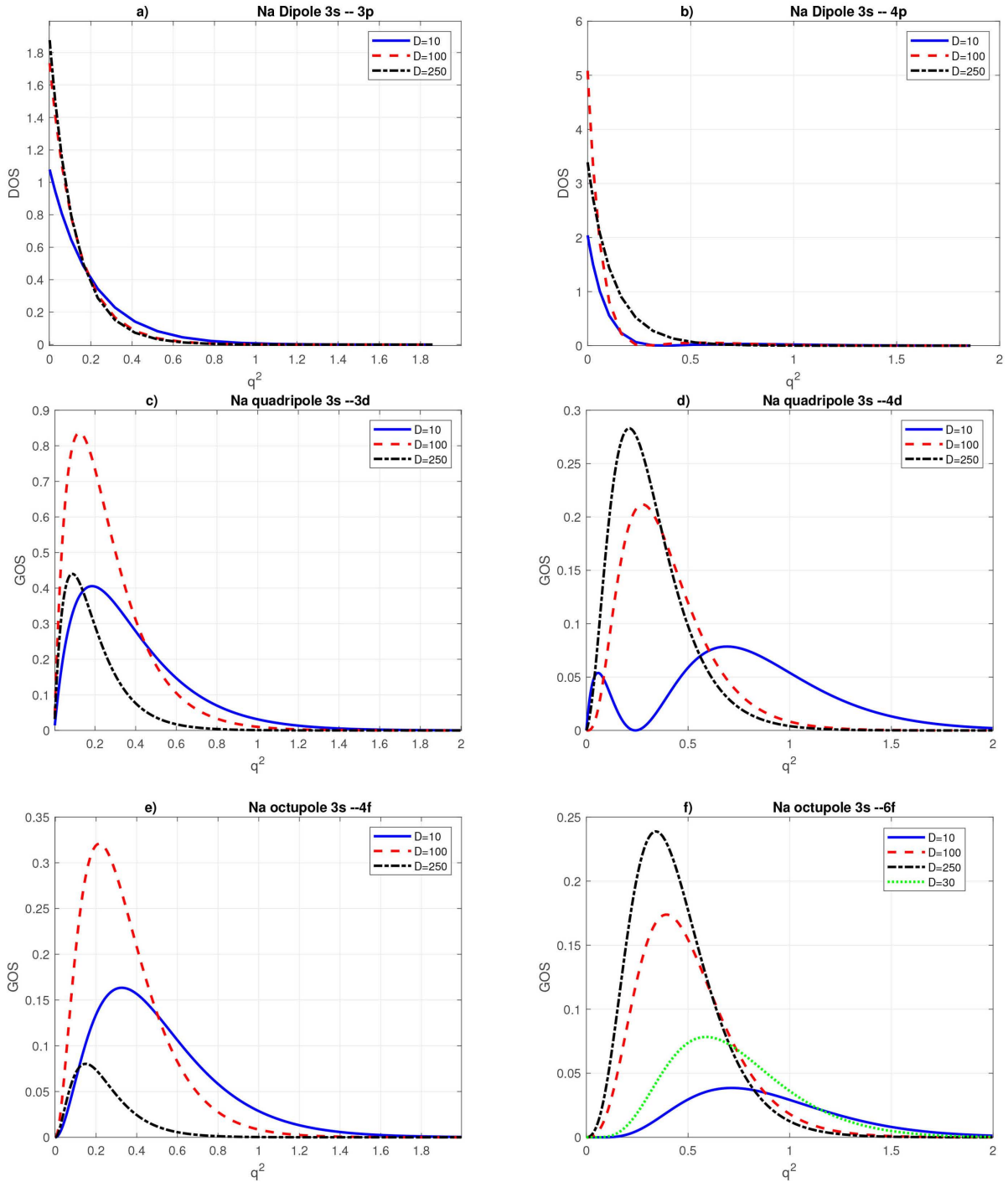

Figure 1. GOS of plasma-immersed sodium atom modeled by MGPM potential with $a=1$, $b=0.5$, $R=25$ and three different D -values.

Wiese *et al.* [22]. This experimental value of the oscillator strength and those obtained with $D=10,100$ and 250 differ by 8.96%, 43.39% and 47.66%, respectively. Even in this simple case of comparison, the purpose may be useful example to show the influence of quantum plasma modelled by MGPM potential on the oscillator strength of the atomic transition. The important observation in

Figure 1(b) is that the absolute values of DOS $3s \to 3s^0 4p$ transition for $D = 100$ are smaller than those determined in the case of $D = 250$ when $q^2 \le 0.0591279$ otherwise the situation is reversed. The explanation can be the poor overlap between initial and final state wavefunctions in the small q^2 region which caused by their broadening to larger radius. The DOS for the excitation to $3s^0 4p$ with $D = 10$ reaches the value of 2.04029 while in the cases of $D = 100$ and 250, it becomes 5.08345 and 3.39021, respectively. For the purpose of comparison, it is also appropriated to report the oscillator strength with values of 0.01420, 0.01423 and 0.015 for Martinez-Flores [8], Qi *et al.* [8] and Regat *et al.* [23], calculated results in free sodium cases. These results obtained for the previous work of other authors and also the oscillator strength with value of 0.0142 measured by Wiese *et al.* [22] are smaller than our numerical data of oscillator strength $3s \to 3s^0 4p$ transition presented here for the screened cases. The difference between this measured value close to the theoretical ones of references [8] [10] [23] quoted above and those calculated with $D = 10,100$ and 250 is around 99.30%, 99.72% and 99.56%, respectively. This high difference arises a more pronounced screening effects on the DOS for $3s \to 3s^0 4p$ transition compared to those affecting the DOS for $3s \to 3s^0 3p$ transition. The quadrupole GOS for the excitations to $3s^0 3d$ and $3s^0 4d$ are shown in the **Figure 1(c)** and **Figure 1(d)**, respectively. All quadrupole GOS curves of the **Figure 1(c)** obtained with $D = 10$, 100 and 250 for the transition $3s \to 3s^0 3d$ have the same shape contrary to the case of transition $3s \to 3s^0 4d$, the profile of quadrupole GOS for $D = 10$ is different to those calculated with $D = 100$ and 250, presenting the similar profile in **Figure 1(d)**. The GOS for $3s \to 3s^0 3d$ quadrupole transition in **Figure 1(c)** are characterized by one maximum with value of 0.405512 at $q^2 = 0.18763$ for $D = 10$, 0.836713 at $q^2 = 0.124724$ for $D = 100$ and 0.439917 at $q^2 = 0.019074$ for $D = 250$. As been clearly given here, the maximum of the quadrupole GOS for $D = 250$ is a factor 0.5238 times lower than that of quadrupole GOS for $D = 100$ and also 1.0848 times higher than the maximum one obtained in the case of $D = 10$. Note that for $D = 100$ and 250 the reason for reduction in GOS's amplitude may be attributed to the poor overlap which causes by the competition between the positive and negative portions within the integrand of the transition matrix element. As seen in **Figure 1(c)**, the peak of quadrupole GOS's curve shifts towards a small squared momentum transfer as a result of 10, 100, 250 increment in D. It is clear from **Figure 1(d)**, the GOS's curves for the excitation to $3s^0 4d$ have a maximum with value 0.28298 at $q^2 = 0.214519$ for $D = 250$ and 0.211681 at $q^2 = 0.273699$ for $D = 100$. For $D = 10$, we see that apart from the first maximum GOS with value 0.0538564 at $q^2 = 0.0591279$, the effects of the screening parameter D induced a quadrupole GOS's minimum at $q^2 = 0.243209$ followed by its second maximum with value 0.0785862 at $q^2 = 0.694159$. The reason for the appearance of these extrema might be related to the nodal structure of radial wavefunctions for which we obtained their product with the spherical Bessel

function generating two favorable overlap regions. As observed in **Figure 1(d)**, the screening parameter D have a considerable effect upon the quadrupole GOS for excitation to $3s^0 4d$, reducing the height of the maxima curves as D decreases. **Figure 1(e)** shows the results of the octupole GOS at D values 10, 100 and 250 for the excitation to $3s^0 4f$ while in **Figure 1(f)** we draw the calculated results of the GOS of the $3s \to 3s^0 6f$ octupole transition for all D values given above as well as introducing additional D value equals 30. All the octupole GOS curves in **Figure 1(e)** have one maximum with value 0.163423 at $q^2 = 0.340078$ for $D = 10$, 0.320901 at $q^2 = 0.214519$ for $D = 100$ and 0.0802693 around $q^2 = 0.146813$ for $D = 250$. Visibly in **Figure 1(e)**, the maximum GOS for $D = 100$ is more important than the calculated one in the case of $D = 10$ which is greater than that found for $D = 250$. This mixed trend in the variation GOS amplitude with increasing D might be caused by a change in dominance of either overlap between initial and final state radial wavefunctions. For each GOS's curve of the octupole transition $3s \to 3s^0 6f$ in **Figure 1(f)**, we observe the same shape of the GOS's curves with the appearance of one maximum with value 0.0384996 at $q^2 = 0.710923$ for $D = 10$, 0.0783319 at $q^2 = 0.582417$ for $D = 30$, 0.173826 at $q^2 = 0.388331$ for $D = 100$ and 0.238803 at $q^2 = 0.340078$ for $D = 250$. **Figure 1(f)** shows that, as D increases, there is an increase of the octupole GOS amplitude for excitation to $3s^0 6f$. As a consequence already been mentioned in the references [10] [24] [25], with the increase of D, GOS for octupole excitations to $3s^0(4f, 6f)$ are broadened and shift in position towards higher values of q^2.

3.2. As a Function of *b*

With the computed radial wavefunctions of Bahar in the case of MGPM potential with $a = 1$, $D = 80$ and three different b-values, the calculation of the dipole oscillator strength for the excitations to $3s^0(3p, 4p)$, the quadrupole and octupole GOS for the excitations to $3s^0(3d, 4d)$ and $3s^0(4f, 6f)$ respectively, has also been performed by using the Equation (8). In order to exhibit perturbative effects modeled by the shielding parameter b, we represent in **Figure 2**, the dipole and generalized oscillator strengths as a function of squared momentum transfer of all considered transitions. The dipole oscillator strengths for the transitions $3s \to 3s^0 3p$ and $3s \to 3s^0 4p$ are been plotted respectively in the **Figure 2(a)** and **Figure 2(b)** while the present calculated values of the quadrupole GOS for the transitions $3s \to 3s^0 3d$ and $3s \to 3s^0 4d$ are been reported in **Figure 2(c)** and **Figure 2(d)**, respectively. The octupole GOS for the transitions $3s^0 \to 3s^0 4f$ and $3s^0 \to 3s^0 6f$ are also given respectively in **Figure 2(e)** and **Figure 2(f)**. The inset graphs in this **Figure 2** show in detail the behavior of present calculated dipole and GOS for each curve at study range of squared momentum transfer q^2. It is seen that for all given shielding parameters, the curves depicting the dipole and generalized oscillator strength converge to

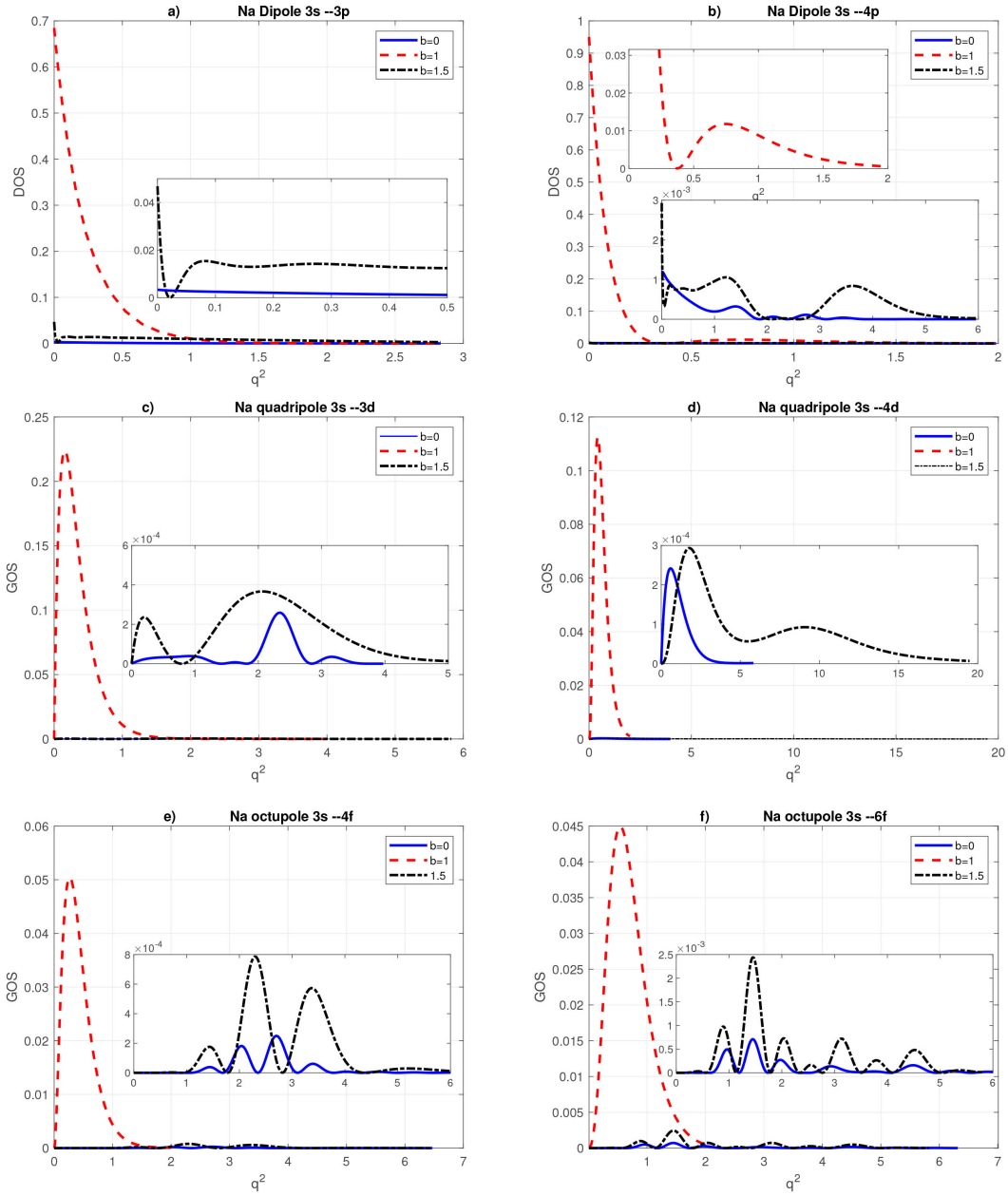

Figure 2. GOS of plasma-immersed Na atom modeled by MGPM potential with $a=1$, $D=80$, $R=25$ and three different b-values.

zero when going from a larger squared momentum transfer q^2. This may be due to a limit momentum transfer determined by the uncertainty principle which atomic electrons cannot receive up without recoiling out of the atom. The panels of **Figure 2** show the behavior of the multipole GOS of the transitions for $\ell=1,2$ and 3 as $b=0,1$ and 1.5. We can see in the panels of this second figure that the dipole and generalized oscillator strength amplitudes for $b=0$ and 1.5 are so small than the other ones obtained when $b=1$. As seen in the case $b=1$, the oscillator strength $3s\to 3s^0 3p$ dipole transition is 0.684678 while the value oscillator strength of $3s\to 3s^0 4p$ dipole transition is 0.95011. The oscillator

strength for the transition $3s \to 3s^0 3p$ is 0.00333538 when b takes the value zero while it becomes 0.0467985 in the case of $b = 1.5$. Our work gives also the oscillator strength of $3s \to 4p$ transition with value 0.00119312 for $b = 0$ while in the case of $b = 1.5$, we obtain the value 0.00293102 of the dipole oscillator strength (DOS) as $q^2 \to 0$. In the inset graph of **Figure 2(a)**, peculiarities are noted in the DOS for $b = 0$ and 1.5 in contrast to the screening parameter $b = 1$, It can be seen that their profile is remarkably different as q^2 increases. When shielding parameter $b = 1$, the DOS value $3s \to 3s^0 3p$ transition decrease continuously as the squared momentum transfer moves to the greater values. For $b = 0$ and 1.5, even there is the decrease, we note also the oscillation of the DOS profile. we observe in **Figure 2(b)** for the case of $b = 0,1.5$ the similar behavior of the DOS $3s \to 3s^0 4p$ to that for $3s \to 3s^0 3p$ DOS's of **Figure 2(a)** in the cases $b = 0,1.5$. This peculiar behavior DOS found for $b = 0$ may be due to the fact that the fluctuation of the wavefunctions which are obtained by using the model potential including both cosine term and spherical encompasement effect. This situation is more pronounced for $b = 1.5$. It may be the consequence of the combination of the facts just quoted above and the perturbative effect through plasma shielding parameter b. As one can note from **Figure 2(b)** in the case $b = 1$, the DOS $3s \to 4p$ has also qualitatively similar behavior to that for $3s \to 3p$ DOS's of **Figure 2(a)** when b takes a same value of 1 except the maximum clearly shown by the inset graph in the present calculated squared momentum transfer region of 0.4 - 2. The calculations of the quadrupole GOS $3s \to 3s^0 (3d, 4d)$ transitions for $b = 1$, give in **Figure 2(c)** and **Figure 2(d)** the curves with one maximum before they decrease until achieving zero around $q^2 = 2$ a.u. The position of this GOS maximum is around $q^2 = 0.154577$ a.u. for the quadrupole excitation to $3s^0 3d$ while for the $3s \to 3s^0 4d$ quadrupole transition, it is near $q^2 = 0.42662$ a.u. In the inset graph of **Figure 2(c)**, we note that, for the case of $b = 0$, the curve of this finding $3s \to 3s^0 3d$ quadrupole GOS transition has a small oscillation before and after the shift maximum position in the region q^2 of 2 - 3 a.u. As been told above, this oscillation may be attributed to cosine term in model potential. For the $3s \to 3s^0 4d$ transition, for $b = 0$, we observe, in the inset graph of **Figure 2(d)** only one peak of the quadrupole GOS curve with little shift position before it decreases towards zero at $q^2 = 5$. For the case of $b = 1.5$, the curves of the GOS for the quadrupole excitations to $3s^0 (3d, 4d)$ present respectively in the inset graph of **Figure 2(c)** and **Figure 2(d)** two maxima and one minimum. The first quadrupole GOS maximum of the $3s \to 3s^0 3d$ and $3s \to 3s^0 4d$ transitions is respectively, in the vicinity of $q^2 = 0.16254$ a.u. and $q^2 = 1.77732$ a.u. We have a GOS minimum of the quadrupole excitation to $3s^0 3d$ at $q^2 = 0.779976$ a.u., while the minimum GOS of the $3s \to 3s^0 4d$ quadrupole transition occurs at $q^2 = 5.49041$ a.u. It is noticed that the position of the second maximum GOS is located around $q^2 = 2.05395$ a.u. for the quadrupole transition $3s \to 3s^0 3d$ and $q^2 = 5.49041$ a.u. for the quadrupole excitation to $3s^0 4d$. In the case of the excitation to $3s^0 3d$, the first quadrupole GOS maximum amplitude is less important than the second one. For the transition $3s \to 3s^0 4d$, the situation is reversed. The explanation can be the

different radial overlap of the wavefunctions, which comes from their decrease in magnitude and their broadening by the enhancement of perturbative effect. From Figure 2(e) and Figure 2(f), the results of the GOS $3s \to 3s^0(4f, 6f)$ octupole transitions show one maximum when their calculations are been done with the radial wavefunctions obtained with the plasma shielding parameter $b = 1$. In the inset graphs of these Figure 2(e) and Figure 2(f), it should be point out that the octupole GOS curves acquire the additional maxima which move to the value of q^2 up to 0.5 a.u. Also, it is interesting to note that for $b = 0,1.5$ the octupole GOS for excitation to $3s^0(4f, 6f)$ are represented by oscillatory shape and their values are almost zero in the small squared momentum transfer region. To understand this behavior, it is important to consider the oscillations of the factor $\cos(r/80)$ in the expression model potential in the case of $b = 0$ and the encompassment effect. For $b = 1.5$, this oscillatory structure of the GOS $3s \to 3s^0(4f, 6f)$ octupole transitions may be a consequence of overlapping strong interactions generated by the cosine term and the parameter b term of the model potential which uses in the calculation wavefunctions. It can also be said that the using orbitals overlap with the continuum and can be taken as an indication of the existence of the critical shielding parameter b closes to the value 1.5. This shows that the shielding parameter b has significance role in the modification of the dipole and generalized oscillator strengths of atomic sodium. Since b is one of the plasma screening parameters inside the potential which uses to model some effects, it should be also indicated to investigate the influence of the parameter a on the same dipole and generalized oscillator strengths.

3.3. As a Function of *a*

After showing the influence of b on the GOS, this dipole and generalized oscillator strength is also investigated dependent on the plasma shielding parameter a. The $3s \to 3s^0(3p, 4p, 3d, 4d, 4f, 6f)$ computed GOS data are obtained by using the radial wavefunctions calculated for $b = 1$, $D = 80$, $R = 25$ and different values of a which are $a = 0,5$ and 10. The computed results of these cases are presented in Figure 3. The present calculations demonstrate that the dipole and generalized oscillator strength tend to zero at large values of the squared momentum transfer. Besides the reason which has been reported above, this situation can also be explained by the variation of the radial wavefunctions for high radius of the atomic electron. Figure 3 shows the variation of the dipole oscillator strength of the $3s \to 3s^0 3p$ transition for $a = 0,5$ and 10 while Figure 3(b) depicts the DOS of the transition $3s \to 3s^0 4p$ for same the values of a. The pictures of Figure 3(a) and Figure 3(b) for the dipole excitations to $3s^0(3p, 4p)$ have qualitatively similar behavior except that's obtained when $a = 5$, for the $3s \to 3s^0 3p$ transition and shown in the inset graph of Figure 3(a). It is also seen from this figure without considering the inset graph, this $3s \to 3s^0 3p$ GOS picture is not clearly appeared because the magnitude difference in plot is negligible. Just as in the inset graph of this figure, the $3s \to 3s^0 3p$ GOS presents a maximum value of order of 0.000191 at

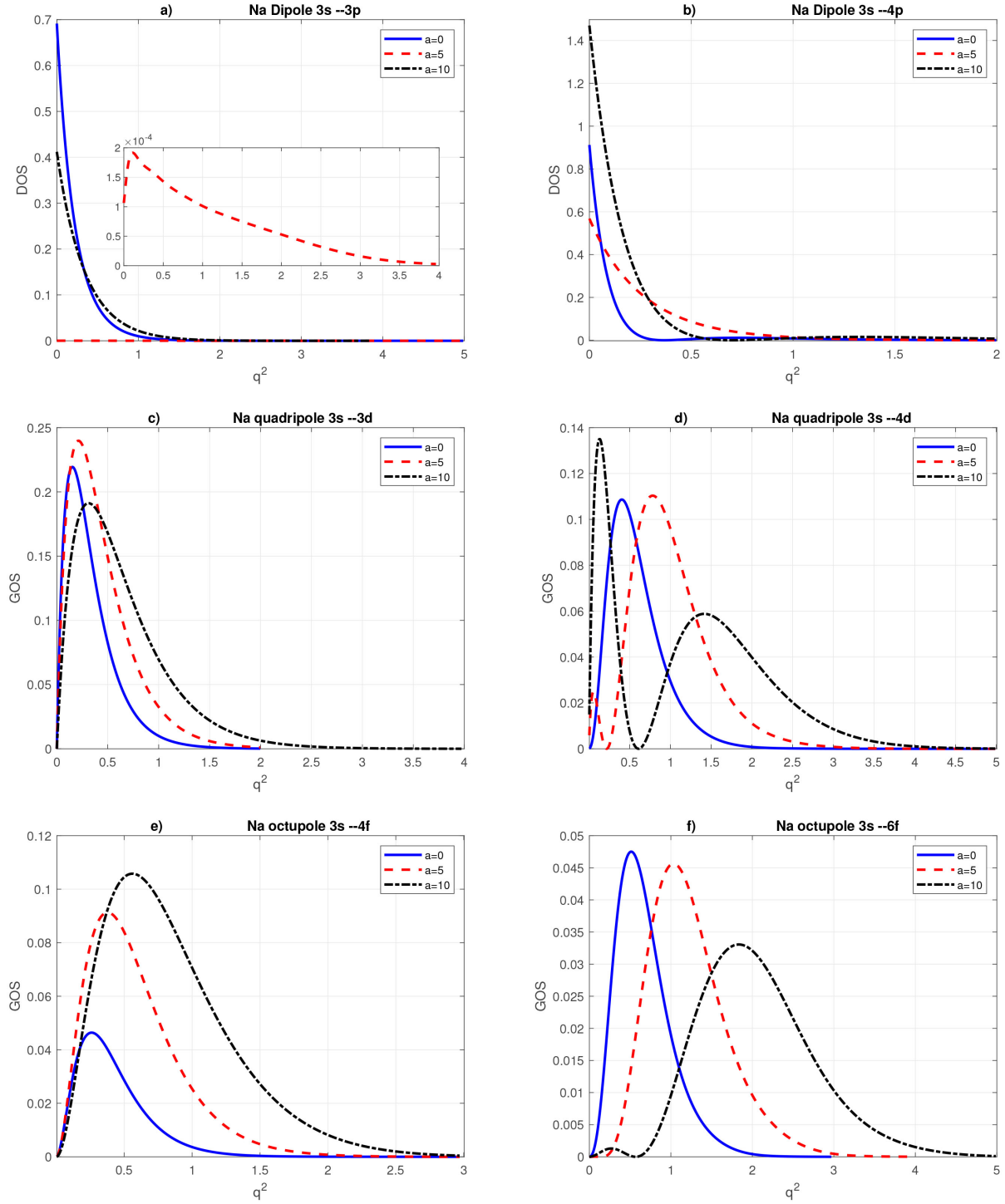

Figure 3. GOS of plasma-immersed sodium atom modeled by MGPM potential with $b=1$, $D=80$, $R=25$ and three different a -values.

$q^2=0.10242$, not counting the value at $q^2\to 0$. This value corresponding the limiting behavior of the DOS as $q^2\to 0$ is our calculated oscillator strength which equals 0.0001065. In this specific case where $a=5$, for excitation to $3s^0 3p$, the behavior of the DOS reflects first as an increase and then as a decrease.

This may be attributable to the momentum distribution character of the wavefunctions of the initial and final states as a result of the cosine term in model potential in this value of $R=25$. In the limit of zero squared momentum transfer, the oscillator strength of the dipole transition $3s \to 3s^0 3p$ is 0.691489 for $a=0$ and 0.411231 for $a=10$. After those values obtained when q^2 tends towards zero, the DOS decrease with increasing q^2. This **Figure 3(a)** shows that the DOS values calculated in the case of $a=0$ are above the data obtained with $a=10$ in the region $q^2 \le 0.314901$ a.u. In the q^2 region of 0.314901−2 a.u, the results of our calculations in the case of $a=10$ lie above the results found by considering the parameter a equals to zero. It may be explained by the fact that the stronger screening effects are altered the spatial overlap between initial and final states which leads here to various overlapping scenarios. Considering **Figure 3(b)** which are been plotted the results of the dipole $3s \to 4p$ transition, it shows that the amplitude DOS for $a=5$ is not negligible than those obtained in the cases of $a=0$ and 10. The explanation may be due by the fact that the effect of the plasma screening on the $4p$ state is less destructive in the overlap with $3s$ state. The present calculation gives the DOS transition $3s \to 3s^0 4p$ reaching an oscillator strength with value of 0.912101 a.u for $a=0$, 0.568102 a.u for $a=5$ and 1.47011 a.u for $a=10$. The curve obtained from computed data with $a=10$ decreases as q^2 increases and remains above that one depicting the results for $a=0$. This is the case for $a=5$ except in squared momentum transfer $q^2 \ge 0.291942$ a.u where the DOS values for $a=10$ are less important than those calculated with $a=5$. This lower DOS, for $a=10$ may be attributed to the less spatial overlap at large q^2 make by the radial wavefunctions which spread out with the increment of the shielding parameter a because of more repulsive effective potential. The GOS for screened cases with the parameter $a=0,5,10$ in **Figure 3(c)** of the quadrupole transition $3s \to 3s^0 3d$ and in **Figure 3(e)** of the octupole transition $3s \to 3s^0 4f$ are characterized by one maximum for all q^2 values considered. Thus, as seen from **Figure 3(c)** and **Figure 3(e)** for all of these same values of a, the GOS profile is similar for the quadrupole transition $3s \to 3s^0 3d$ and for the octupole transition $3s \to 3s^0 4f$. It arises for the values of $a=5$ and 10 the GOS in **Figure 3(d)** of the quadrupole excitation to $3s^0 4d$ has two maxima and one minimum while the GOS's curve obtained with $a=0$ presents only one maximum. In **Figure 3(f)**, we note also that the octupole GOS of the $3s \to 3s^0 6f$ transition has one maximum apart from the second maximum appears as early and followed by the minimum in the case of $a=10$. It is evident from **Figure 3(c)** that for $b=1$, $D=80$ and $R=25$ as a increases, the curves of GOS have the same shape. The magnitude GOS's curve of the quadrupole excitation to $3s^0 3d$ for $a=5$ is more important than the GOS amplitude of the case $a=0$ which is also greater than the one obtained for $a=10$. Even has been noted the increase of the quadrupole GOS in the region of $q^2 \le 0.124724$ a.u, the results for $a=0$ are in accordance with those calculated by taking the value of $a=5$. Above this value

of $q^2 = 0.124724$ a.u, it is also observed that the absolute value of this quadrupole GOS in the case of $a = 5$ are greater than those for $a = 0$. Above their maxima position, we observe a decrease of this GOS until achieving zero around $q^2 = 2$. It is clear for the shielding parameter $a = 10$, this quadrupole GOS for excitation to $3s^0 3d$ increases in the region $q^2 \le 0.124724$ and then decreases to zero as q^2 increases. We note that the absolute values of this quadrupole GOS for $a = 10$ are underestimated those obtained in the cases of $a = 0$ and 5 when q^2 is up to 0.413658. Visibly with the increment of the parameter a, **Figure 3(c)** shows also the shift of the peak curve values of the quadrupole GOS towards greater squared momentum transfer. This leads to make the GOS extend to the larger squared momentum transfer which may be a consequence of the broadening of the radial wavefunctions used in the calculations. For this increment of a parameter from 5 to 10, the calculations have also reduced the maximum of this GOS due to an unfavorable contribution in spatial overlap between these radial wavefunctions. But the increase of the GOS's maximum with the increment of a from 0 to 5 may be explained by the strong spatial overlap of the radial wavefunctions of the initial $3s$ and final $3d$ states which are in the region of radial distance close to coordinate origine. In the present study of the quadrupole excitation to $3s^0 3d$, the maximum GOS for $a = 5$ is 1.0930 larger than that of the one obtained in the case of $a = 0$ which is 2.0287 larger than the corresponding one calculated with $a = 10$. They occur at $q^2 = 0.154577$, 0.214519 and 0.439784 for the cases of $a = 0, 5$ and 10, respectively. From **Figure 3(d)**, we note the large changes in the quadrupole GOS of the transition $3s \to 3s^0 4d$ for $a = 5$ and 10 in comparison with the results display in the case of $a = 0$. These changes are an oscillatory behavior in the quadrupole GOS curves which arises from the oscillations caused by cosine term in more general plasma model potential. That GOS curves are also characterized by set of maxima: one narrow in the small q^2 region and another broad in the large q^2 region while the made calculations in the case of $a = 0$ give the quadrupole GOS with only one broad maximum at $q^2 = 0.400894$. Note that for small q^2 region which have been located these first maxima quadrupole GOS, the oscillatory screening effects rise the amplitude when the a parameter increases. Then, the first maximum of this quadrupole GOS for $a = 10$ is 5.413304 larger than that of the first maximum quadrupole GOS for $a = 5$. For the large q^2 region, our calculations indicated that as the parameter a increases the height of the second maxima of the quadrupole GOS excitation to $3s^0 4d$ decrease. The ratio between the second maximum quadrupole GOS for $a = 10$ and the same calculated in the case of $a = 5$ is 0.53300321. This GOS behavior may be analyzed by the fact that the more general plasma model potential alters the initial and final radial wavefunctions leading to the shift in their spatial overlap and also the creation of two strong overlap regions. So, the increase of the first maximum quadrupole GOS amplitude as the a parameter increases, may be explained by the large radial overlap in the inner distance due

to the $4d$ orbital penetration. The position of the first maximum for quadrupole GOS of the excitation to $3s^0 4d$ is in the vicinity of $q^2 = 0.0591279$ in the case of $a = 5$ and becomes $q^2 = 0.131887$ due to the increment in $a = 10$. The second maximum GOS position found in our calculation when $a = 5$, is at around $q^2 = 0.779976$ while it is near $q^2 = 1.35295$ as a reaches the value of 10. It is also interesting to note that the curve depicting the results of this quadrupole GOS presents the minimum at $q^2 = 0.214519$ for the parameter $a = 5$ and $q^2 = 0.613343$ for the value of $a = 10$. The results are found to exhibit an upward shift on increasing the value of the parameter a, $a = 0,5$ and 10. **Figure 3(e)** shows clearly the GOS values of the octupole $3s \to 3s^0 4f$ transition calculated with the shielding parameter $a = 0,5$ and 10 are both in accordance in the region $q^2 \le 0.18763$. Above this value of q^2, there is always gradual increase of this octupole GOS values with the a parameter increasing, but their values differ. Then, this GOS rise and attains a maximum value before decreasing until achieving an extremely small value in the vicinity of $q^2 = 1.5, 2$ and 3 for the cases $a = 0,5$ and 10, respectively. These maxima GOS values are 0.0463971, 0.0913042 and 0.105775 for $a = 0$, $a = 5$ and $a = 10$, respectively. For the parameter $a = 0$, we find it at $q^2 = 0.263336$, for $a = 5$ at $q^2 = 0.375968$ and for $a = 10$ at $q^2 = 0.567253$. As a result of 0, 5 and 10 in the a parameter, the GOS of the octupole $3s \to 3s^0 4f$ transition increases and their maxima move to the large squared momentum transfer. As observed in **Figure 2(f)**, the $3s \to 3s^0 6f$ octupole transition GOS amplitude decreases with the increment of shielding parameter a, but their maxima positions always shift towards larger q^2 apart from the little maximum appears at $q^2 = 0.273699$ which has been already mentioned above in the case of $a = 10$. In order to emphasize this reverse situation noted in the variation amplitude we can now display the values of the peaks of the GOS curve for the octupole excitation to $3s^0 6f$. The maximum value of the GOS octupole transition $3s \to 3s^0 6f$ for $a = 0$ reaches 0.0475079 and it is slightly higher than the maximum GOS for $a = 5$ with value of 0.045632 which is clearly greater than the value of 0.0330596 corresponding to the maximum GOS value for $a = 10$. Their positions are $q^2 = 0.5086$ for $a = 0$, $q^2 = 1.0265$ for $a = 5$ and $q^2 = 1.83105$ for $a = 10$. The appearance of the little maximum and a minimum at $q^2 = 0.567253$ is a consequence of the oscillations in the initial and final state wavefunctions, and also in the spherical Bessel function which results in an alteration in the negative and positive contribution to the radial function under the integral of the transition matrix element and thus the variation of their overlap. The spherical confinement and the quantum plasma effects affect the wavefunctions and consequently the dipole and generalized oscillator strengths much more the Debye plasma. Among the parameters of the MGPM potential, the b parameter has a far greater influence on the dipole and generalized oscillator strengths than D or a.

4. Conclusions

To conclude, we have studied quantum plasma screening and spherical

confinement effects on the dipole and generalized oscillator strength for sodium atomic excitations to $3s^0(3p,4p,3d,4d,4f,6f)$. The more general plasma model potential which takes account of wide variety and complicated interactions in the plasma environment has been considered in our calculations. The present work calculations have shown that dipole and generalized oscillator strength are very sensitive in quantum plasma and spherical encompassing with radius R. The results show that while the shielding parameter are varied, the dipole and generalized oscillator strength are modified strongly. As a consequence in the behaviour, the negligibility of amplitude difference in plot comes from the oscillation in the DOS and GOS for the case of $b=0$ and 1.5 shown in the inset graph. The increment in D strongly favours dipole $3s \to 3s^0(3p,4p)$ transitions according to the increase values of oscillator strength. This study lets us see also the positions of the quadrupole and octupole GOS maxima shift towards small squared momentum transfer q^2 when D increases, as well as the decrease of the parameter a. With the combined effect of the parameters of the potential and spherical confinement, the GOS dependence on q^2 for multiple strengths $\ell=2,3$ acquires an additional maximum.

Conflicts of Interest

The authors declare no conflicts of interest regarding the publication of this paper.

References

[1] Metcalf, H.J. and Van Der Straten, P. (1999) Laser Cooling and Trapping. Springer.

[2] Zhou, Z., Shi, J., Bi, S., Yan, H., Zhang, J., Pan, K., *et al.* (2023) NLTE Analysis of High-Resolution H-Band Spectra, V: Neutral Sodium. *Universe*, **9**, Article 457. https://doi.org/10.3390/universe9110457

[3] Eviatar, A., Mekler, Y. and Coroniti, F.V. (1976) Jovian Sodium Plasma. *The Astrophysical Journal*, **205**, 622. https://doi.org/10.1086/154319

[4] Han, X., Li, Y., Zhang, H., Yan, J., Li, J. and Voky, L. (2008) R-Matrix Treatment of High-Energy Electron-Impact Excitation Processes: The Generalized Oscillator Strengths for the Na 3s-3p and 2p-3s Transitions. *Physical Review A*, **78**, Article ID: 052702. https://doi.org/10.1103/physreva.78.052702

[5] Han, X.Y., Li, Y.M., Yan, J. and Zhu, L.F. (2009) The Generalized Oscillator Strengths for Na: Monopole, Dipole and Quadrupole Transitions. *Journal of Physics B: Atomic, Molecular and Optical Physics*, **42**, Article ID: 195003. https://doi.org/10.1088/0953-4075/42/19/195003

[6] Chen, Z. and Msezane, A.Z. (2000) Generalized Oscillator Strength for the Na 3s-3p Transition. *Physical Review A*, **61**, Article ID: 030703.

[7] Sahoo, S. and Ho, Y.K. (2006) Photoionization of Li and Na in Debye Plasma Environments. *Physics of Plasmas*, **13**, Article ID: 063301. https://doi.org/10.1063/1.2200290

[8] Qi, Y. and Ning, L. (2014) Dynamic Processes and Polarizability of Sodium Atom in Debye Plasmas. *Physics of Plasmas*, **21**, Article ID: 033301. https://doi.org/10.1063/1.4867060

[9] Das, M. and Pradhan, A.C. (2017) Spectroscopy of Na I and K I Atoms Embedded in

Weakly Coupled Plasma Environment. *Physics of Plasmas*, **24**, Article ID: 112706. https://doi.org/10.1063/1.4986022

[10] Martínez-Flores, C. (2020) Generalized Oscillator Strengths for the Ground State $[2p^6 3s]^2S$ of Sodium Atom Embedded in a Plasma Medium. *Chemical Physics*, **535**, Article ID: 110759. https://doi.org/10.1016/j.chemphys.2020.110759

[11] Bethe, H.A. and Jackiw, R. (1986) Intermediate Quantum Mechanics. 3rd Edition, The Benjamin Cummings Publishing Company.

[12] Bethe, H. (1930) Zur Theorie des Durchgangs schneller Korpuskularstrahlen durch Materie. *Annalen der Physik*, **397**, 325-400. https://doi.org/10.1002/andp.19303970303

[13] Amusia, M.Y. and Chernysheva, L.V. (1997) Computation of Atomic Processes: A Handbook for ATOM Programs. Institute of Physics Publishing.

[14] Bahar, M.K. (2022) Manipulating the Orbital Charge-Currents of Compressed Li and Na Atom Embedded in Quantum Plasma. *Chemical Physics*, **557**, Article ID: 111484. https://doi.org/10.1016/j.chemphys.2022.111484

[15] Gomis, L., Diatta, C., Tall, M.S., Faye, I.G., Gomis, R., Diouf, Y., *et al.* (2024) Velocity Form Calculations of Generalized Oscillator Strengths for 3s→ (3p, 4p, 5p, 6p) Dipole Transitions of Atomic Sodium in Debye Plasma. *Open Journal of Applied Sciences*, **14**, 1512-1529. https://doi.org/10.4236/ojapps.2024.146101

[16] Diatta, C., Gomis, L., Faye, I.G., Martínez-Flores, C., Tall, M.S., Diouf, Y., *et al.* (2024) Generalized Oscillator Strength of Valence-Shell Excitations of Atomic Sodium in Debye Plasma within the Frame of Two Various Methods. *Open Journal of Applied Sciences*, **14**, 3649-3667. https://doi.org/10.4236/ojapps.2024.1412239

[17] Amusia, M.Y., Chernysheva, L.V. and Yarzhemsky, V. (2012) Handbook of Theoretical Atomic Physics Data for Photon Absorption, Electron Scattering, and Vacancies Decay. Springer.

[18] Pindzola, M.S. and Kelly, H.P. (1975) Comparison of the Acceleration, Length, and Velocity Forms of the Dipole Operator in Photoionization Calculations. *Physical Review A*, **12**, 1419-1424. https://doi.org/10.1103/physreva.12.1419

[19] Amusia, M.Y. (1990) Atomic Photoeffect. Plenum.

[20] Amusia, M.Y., Cherepkov, N.A., Živanović, D. and Radojević, V. (1976) Photoabsorption for Helium, Lithium, and Beryllium Atoms in the Random-Phase Approximation with Exchange. *Physical Review A*, **13**, 1466-1474. https://doi.org/10.1103/physreva.13.1466

[21] Li, H.W. and Kar, S. (2012) Polarizabilities of Li and Na in Debye Plasmas. *Physics of Plasmas*, **19**, Article ID: 073303. https://doi.org/10.1063/1.4739229

[22] Wiese, W.L., Smith, M.W. and Glennon, B.M. (1969) Atomic Transition Probabilities (NSRDS?NBS). U.S. Government Publishing Office.

[23] Rérat, M., Mérawa, M. and Honvault-Bussery, B. (1998) *Ab Initio* Calculations of Dipole Polarizabilities of Na and K in Their 3^2D-State and Determination of Long-Range Coefficients for S + D Molecular States of Na_2, K_2, and NaK. *The Journal of Chemical Physics*, **109**, 7246-7251. https://doi.org/10.1063/1.477358

[24] Martínez-Flores, C. and Cabrera-Trujillo, R. (2018) Dipole and Generalized Oscillator Strength Derived Electronic Properties of an Endohedral Hydrogen Atom Embedded in a Debye-Hückel Plasma. *Matter and Radiation at Extremes*, **3**, 227-242. https://doi.org/10.1016/j.mre.2018.05.001

[25] Qi, Y.Y., Wu, Y., Wang, J.G. and Qu, Y.Z. (2009) The Generalized Oscillator Strengths of Hydrogenlike Ions in Debye Plasmas. *Physics of Plasmas*, **16**, Article ID: 023502. https://doi.org/10.1063/1.3073675